

Supplementary Materials

Unconstrained and X-ray constrained Extremely Localized Molecular Orbitals: analysis of the reconstructed electron density

Leonardo H. R. Dos Santos^a, Alessandro Genoni^{b,c*} and Piero Macchi^a

^a Department of Chemistry and Biochemistry, University of Bern, Freiestrasse 3, Bern, CH-3012, Switzerland

^b CNRS, Laboratoire SRSMC, UMR 7565, Vandoeuvre-lès-Nancy, F-54506, France

^c Université de Lorraine, Laboratoire SRSMC, UMR 7565, Vandoeuvre-lès-Nancy, F-54506, France

* Correspondence email: Alessandro.Genoni@univ-lorraine.fr

Figure S1. Experimental residual density plots for glycylglycine after the MM2 multipole refinement. All reflections are included. The step size is $0.05 \text{ e.}\text{\AA}^{-3}$. Full, blue contours are positive. Dashed, red contours are negative.

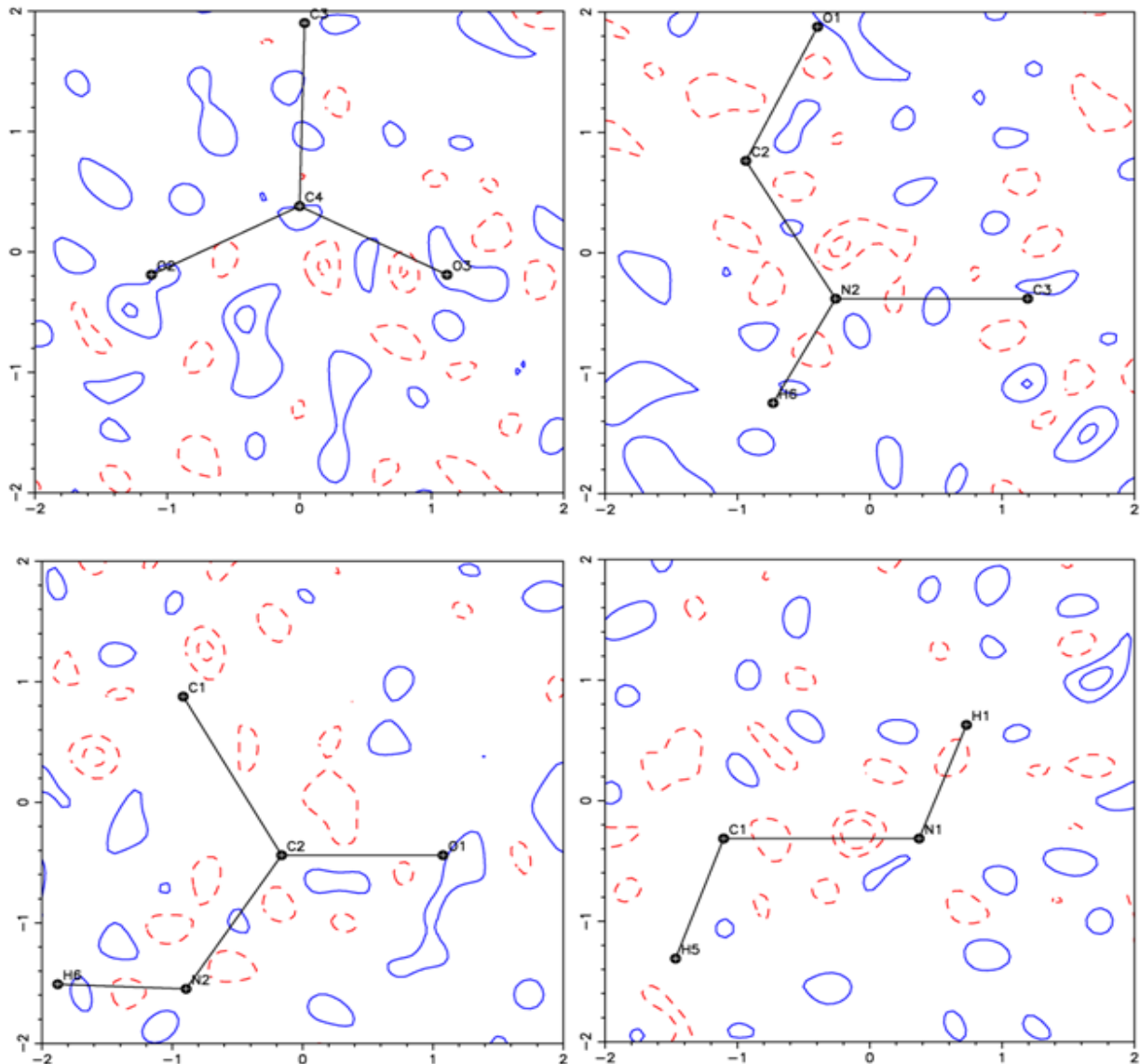


Figure S2. Variation of scale factor ($\Sigma F_o^2 / \Sigma F_c^2$) with resolution (for data averaged within 0.05 Å⁻¹ intervals) from the experimental MM2 multipole refinement of glycylglycine.

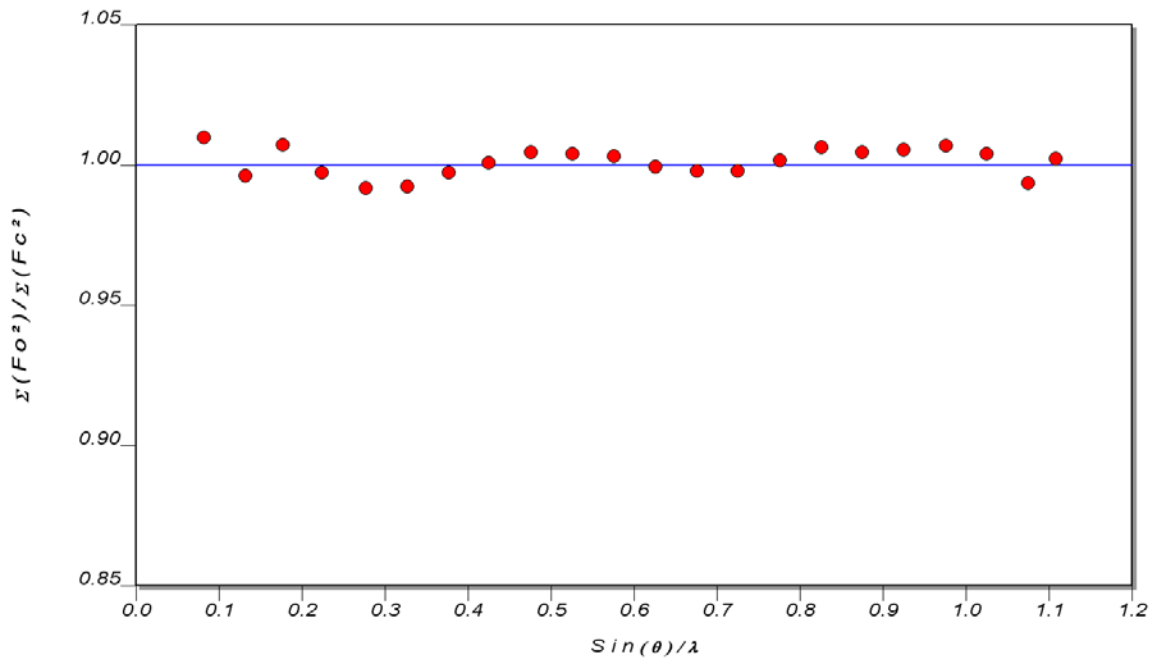


Figure S3. Normal probability plot from the experimental MM2 multipole model refinement of glycylglycine.

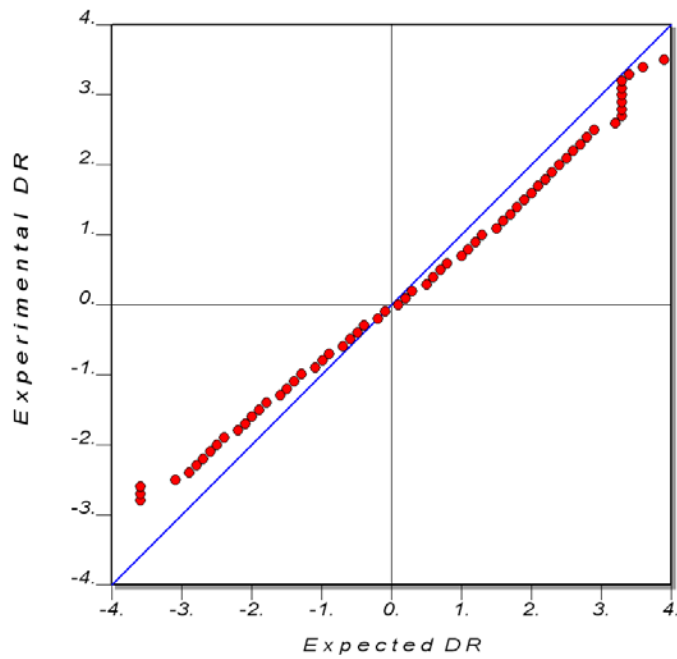


Figure S4. Residual electron density and fractal dimension distributions from the experimental MM2 multipole model refinement of glycylglycine.

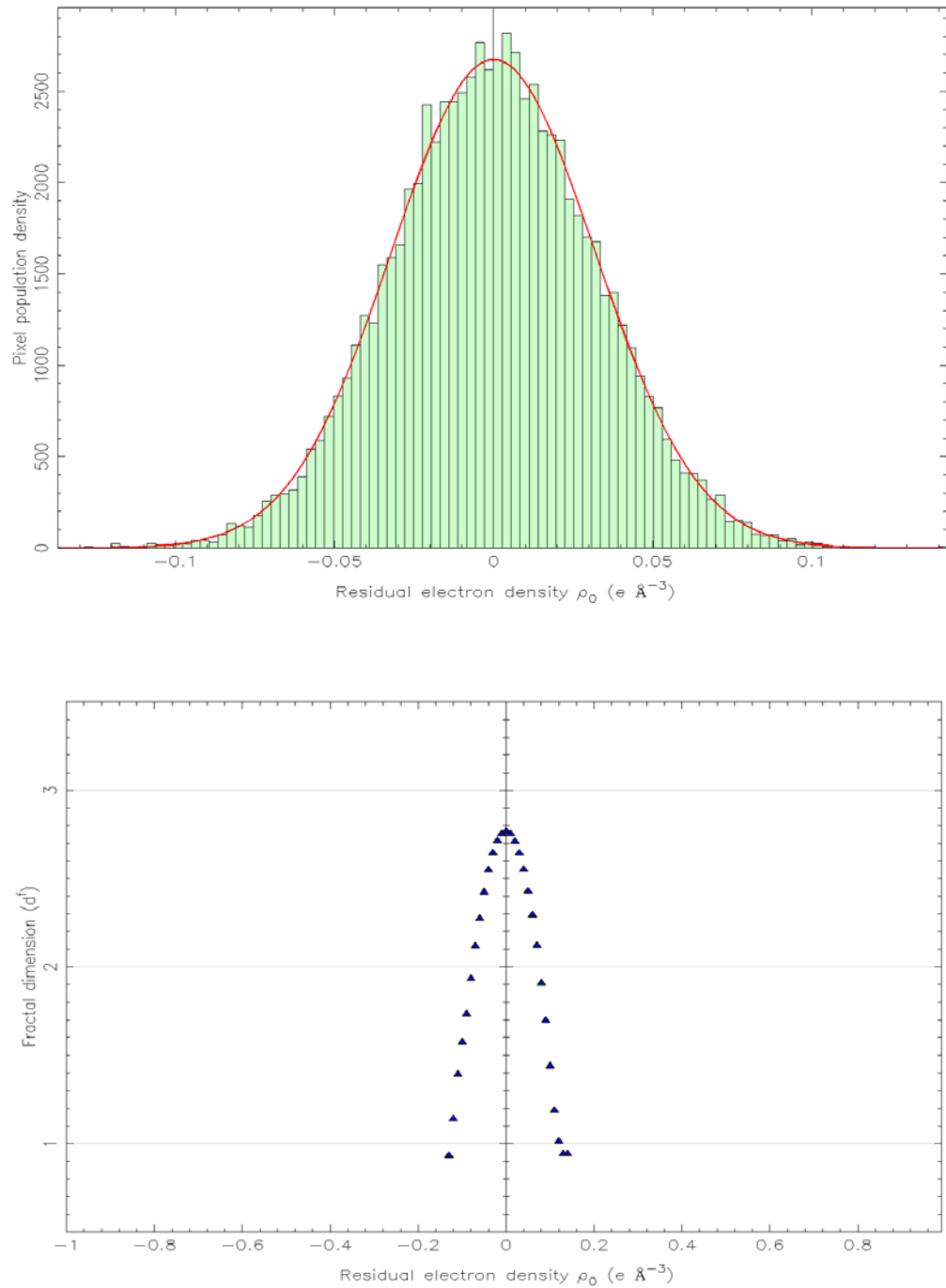


Table S1. Atomic monopole populations (P_v), κ and κ' parameters for the multipole-fitted electron densities.

	O1	O2	O3	N1	N2	C1	C2	C3	C4	H1	H2	H3	H4	H5	H6	H7	H8
$\rho^{MM/XC}$																	
P_v	6.23(3)	6.30(3)	6.30(3)	5.34(6)	5.07(4)	4.14(7)	4.12(5)	4.20(8)	4.14(6)	0.67(2)	0.70(2)	0.69(2)	0.82(3)	0.87(3)	0.76(2)	0.84(3)	0.83(3)
κ	0.986(2)	0.983(2)	0.982(2)	0.981(4)	0.996(3)	0.996(5)	0.993(4)	0.993(5)	0.981(5)	1.22(2)	1.22(2)	1.22(2)	1.22(2)	1.22(2)	1.22(2)	1.22(2)	1.22(2)
κ'	0.99(4)	0.85(3)	0.81(4)	0.88(2)	0.95(3)	0.96(2)	0.90(2)	0.90(2)	0.92(2)	1.29	1.29	1.29	1.29	1.29	1.29	1.29	1.29
$\rho^{MM/P-B3LYP/6-31G(2d,2p)}$																	
P_v	6.30	6.37	6.39	5.10	5.06	3.98	4.00	3.98	3.92	0.77	0.80	0.78	0.89	0.92	0.86	0.94	0.97
κ	0.984	0.982	0.980	0.994	0.998	1.009	1.009	1.016	1.011	1.18	1.18	1.18	1.18	1.18	1.18	1.18	1.18
κ'	1.11	1.11	1.13	0.86	1.03	0.93	0.89	0.94	0.92	1.29	1.29	1.29	1.29	1.29	1.29	1.29	1.29
$\rho^{MM/ELMO/6-31G}$																	
P_v	6.40	6.47	6.46	5.14	5.24	3.89	3.84	3.77	3.89	0.76	0.80	0.78	0.90	0.91	0.81	0.97	0.98
κ	0.972	0.967	0.968	0.993	0.985	1.013	1.015	1.023	1.011	1.22	1.22	1.22	1.22	1.22	1.22	1.22	1.22
κ'	0.95	0.90	0.92	0.81	0.86	0.90	0.90	0.93	0.88	1.29	1.29	1.29	1.29	1.29	1.29	1.29	1.29
$\rho^{MM/ELMO/6-31G(d,p)}$																	
P_v	6.34	6.42	6.41	4.99	5.05	3.71	4.06	3.67	4.06	0.79	0.83	0.81	0.96	0.97	0.88	1.02	1.03
κ	0.972	0.967	0.967	0.987	0.984	1.004	0.979	1.010	0.972	1.18	1.18	1.18	1.18	1.18	1.18	1.18	1.18
κ'	1.07	1.03	1.06	0.84	0.94	0.97	0.90	0.99	0.89	1.29	1.29	1.29	1.29	1.29	1.29	1.29	1.29
$\rho^{MM/ELMO/cc-pVDZ}$																	
P_v	6.34	6.43	6.43	5.05	5.08	3.67	3.97	3.66	3.94	0.79	0.84	0.82	0.98	0.99	0.90	1.05	1.05
κ	0.973	0.968	0.968	0.979	0.981	1.001	0.985	1.006	0.981	1.15	1.15	1.15	1.15	1.15	1.15	1.15	1.15
κ'	1.03	1.00	1.03	0.81	0.93	0.89	0.88	0.92	0.88	1.29	1.29	1.29	1.29	1.29	1.29	1.29	1.29

Table S1. *Cont.*

	O1	O2	O3	N1	N2	C1	C2	C3	C4	H1	H2	H3	H4	H5	H6	H7	H8
$\rho^{MM/XC-ELMO/6-31G}$																	
P_v	6.50	6.60	6.58	5.12	5.21	4.00	3.73	3.98	3.65	0.72	0.77	0.76	0.89	0.91	0.76	0.93	0.91
κ	0.967	0.965	0.966	0.995	0.987	1.009	1.007	1.008	1.015	1.22	1.22	1.22	1.22	1.22	1.22	1.22	1.22
κ'	0.72	0.72	0.71	0.83	0.77	0.91	0.98	0.90	1.00	1.29	1.29	1.29	1.29	1.29	1.29	1.29	1.29
$\rho^{MM/XC-ELMO/6-31G(d,p)}$																	
P_v	6.37	6.42	6.44	5.07	5.07	3.85	4.02	3.77	4.04	0.74	0.78	0.78	0.92	0.94	0.84	0.99	0.98
κ	0.970	0.969	0.967	0.988	0.985	0.998	0.982	1.002	0.979	1.18	1.18	1.18	1.18	1.18	1.18	1.18	1.18
κ'	1.00	0.95	1.03	0.85	0.91	0.97	0.90	0.97	0.90	1.29	1.29	1.29	1.29	1.29	1.29	1.29	1.29
$\rho^{MM/XC-ELMO/cc-pVDZ}$																	
P_v	6.36	6.42	6.44	5.12	5.08	3.83	3.97	3.75	3.99	0.74	0.78	0.78	0.93	0.95	0.85	1.01	1.00
κ	0.971	0.969	0.968	0.982	0.983	0.996	0.984	1.000	0.982	1.15	1.15	1.15	1.15	1.15	1.15	1.15	1.15
κ'	0.94	0.90	0.96	0.81	0.89	0.90	0.88	0.92	0.89	1.29	1.29	1.29	1.29	1.29	1.29	1.29	1.29

Figure S5. Three-dimensional plot of the electron density difference $\rho^{\text{XC-ELMO}} - \rho^{\text{ELMO}}$ for the cc-pVDZ basis-set. The isosurface value is set to 0.005 au, with negative isosurfaces in red and positive isosurfaces in blue.

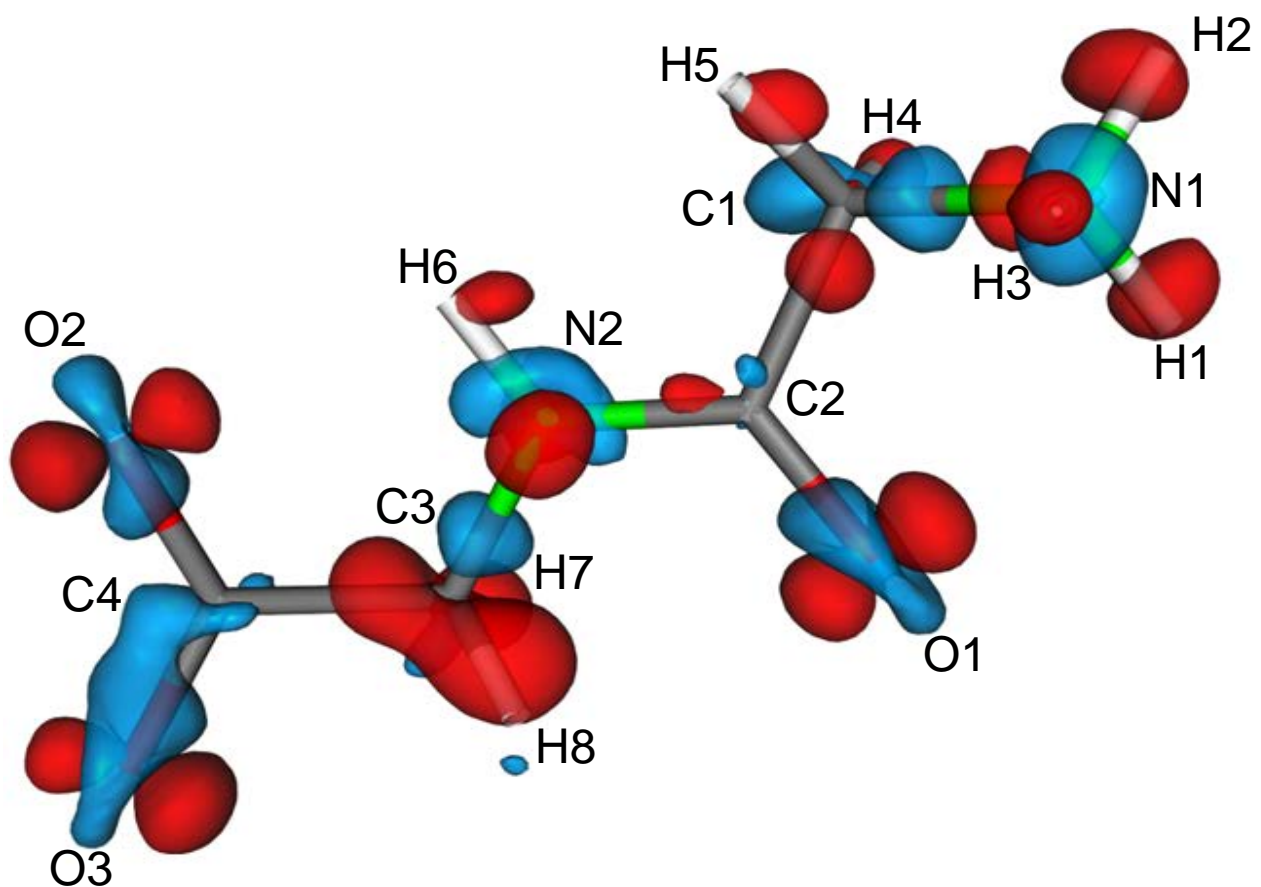


Table S2. Integrated net atomic charges (au) associated with the glycylglycine electron densities obtained from unconstrained and constrained ELMO calculations and from the periodic B3LYP/6-31G(2d,2p) computation. Bar-graphs are shown in Fig. 7 of the main text.

	$\rho^{P-B3LYP}$	ρ_{6-31G}^{ELMO}	$\rho_{6-31G(d,p)}^{ELMO}$	$\rho_{cc-pVDZ}^{ELMO}$	$\rho_{6-31G}^{XC-ELMO}$	$\rho_{6-31G(d,p)}^{XC-ELMO}$	$\rho_{cc-pVDZ}^{XC-ELMO}$
O1	-1.176	-1.133	-1.414	-1.359	-1.217	-1.412	-1.369
O2	-1.210	-1.240	-1.499	-1.447	-1.267	-1.455	-1.410
O3	-1.216	-1.120	-1.467	-1.414	-1.250	-1.443	-1.400
N1	-1.109	-0.995	-1.274	-1.369	-0.920	-1.271	-1.319
N2	-1.163	-1.150	-1.571	-1.547	-1.160	-1.533	-1.507
C1	0.325	0.335	0.482	0.484	0.334	0.457	0.424
C2	1.379	1.314	1.901	1.823	1.439	1.759	1.704
C3	0.420	0.478	0.647	0.601	0.538	0.654	0.614
C4	1.584	1.545	2.109	2.022	1.580	1.949	1.883
H1	0.513	0.511	0.572	0.608	0.514	0.583	0.607
H2	0.519	0.451	0.512	0.549	0.429	0.516	0.538
H3	0.512	0.476	0.535	0.573	0.502	0.558	0.587
H4	0.065	0.077	0.041	0.022	0.077	0.089	0.089
H5	0.053	0.070	0.028	0.020	0.041	0.062	0.061
H6	0.495	0.466	0.518	0.553	0.474	0.546	0.569
H7	0.027	-0.016	-0.071	-0.081	-0.035	-0.015	-0.019
H8	-0.010	0.006	-0.049	-0.040	-0.082	-0.047	-0.053
Σq	0.008	-0.001	-0.001	0.001	-0.001	-0.001	-0.001

Table S3. Atomic dipole moment magnitudes (au) associated with the glycylglycine electron densities obtained from unconstrained and constrained ELMO calculations and from the periodic B3LYP/6-31G(2d,2p) computation. Bar-graphs are shown in Fig. 8 of the main text.

	$\rho^{P-B3LYP}$	ρ_{6-31G}^{ELMO}	$\rho_{6-31G(d,p)}^{ELMO}$	$\rho_{cc-pVDZ}^{ELMO}$	$\rho_{6-31G}^{XC-ELMO}$	$\rho_{6-31G(d,p)}^{XC-ELMO}$	$\rho_{cc-pVDZ}^{XC-ELMO}$
O1	0.368	0.048	0.559	0.469	0.043	0.496	0.440
O2	0.334	0.089	0.488	0.399	0.063	0.444	0.389
O3	0.340	0.071	0.521	0.430	0.032	0.489	0.430
N1	0.180	0.051	0.018	0.097	0.123	0.036	0.107
N2	0.237	0.076	0.361	0.311	0.243	0.324	0.294
C1	0.429	0.482	0.564	0.537	0.436	0.568	0.535
C2	0.660	0.528	0.657	0.628	0.612	0.766	0.738
C3	0.402	0.468	0.569	0.565	0.387	0.513	0.497
C4	0.680	0.532	0.640	0.603	0.566	0.723	0.678
H1	0.124	0.130	0.126	0.133	0.142	0.135	0.142
H2	0.125	0.146	0.144	0.153	0.167	0.160	0.169
H3	0.127	0.138	0.136	0.144	0.130	0.143	0.149
H4	0.079	0.119	0.095	0.089	0.115	0.127	0.126
H5	0.089	0.122	0.096	0.094	0.142	0.135	0.135
H6	0.132	0.145	0.141	0.151	0.160	0.148	0.157
H7	0.092	0.134	0.099	0.100	0.195	0.175	0.177
H8	0.109	0.123	0.088	0.100	0.213	0.173	0.174

Table S4. Molecular dipole moment magnitudes (au) for glycylglycine obtained from the constrained and unconstrained ELMO calculations and from the periodic B3LYP/6-31G(2d,2p) computation. Bar-graphs are shown in Fig. 9 (a) of the main text.

$\rho^{P-B3LYP}$	ρ_{6-31G}^{ELMO}	$\rho_{6-31G(d,p)}^{ELMO}$	$\rho_{cc-pVDZ}^{ELMO}$	$\rho_{6-31G}^{XC-ELMO}$	$\rho_{6-31G(d,p)}^{XC-ELMO}$	$\rho_{cc-pVDZ}^{XC-ELMO}$
11.337	10.832	9.948	9.909	11.195	10.762	10.781

Figure S6. Deformation electron density plot for glycylglycine calculated from (a) unconstrained ($\rho^{MM/ELMO} - \rho^{IAM}$) and (b) constrained ($\rho^{MM/XC-ELMO} - \rho^{IAM}$) cc-pVDZ ELMO wave functions. The isosurface value is set to 0.02 au, with negative isosurfaces in red and positive isosurfaces in blue.

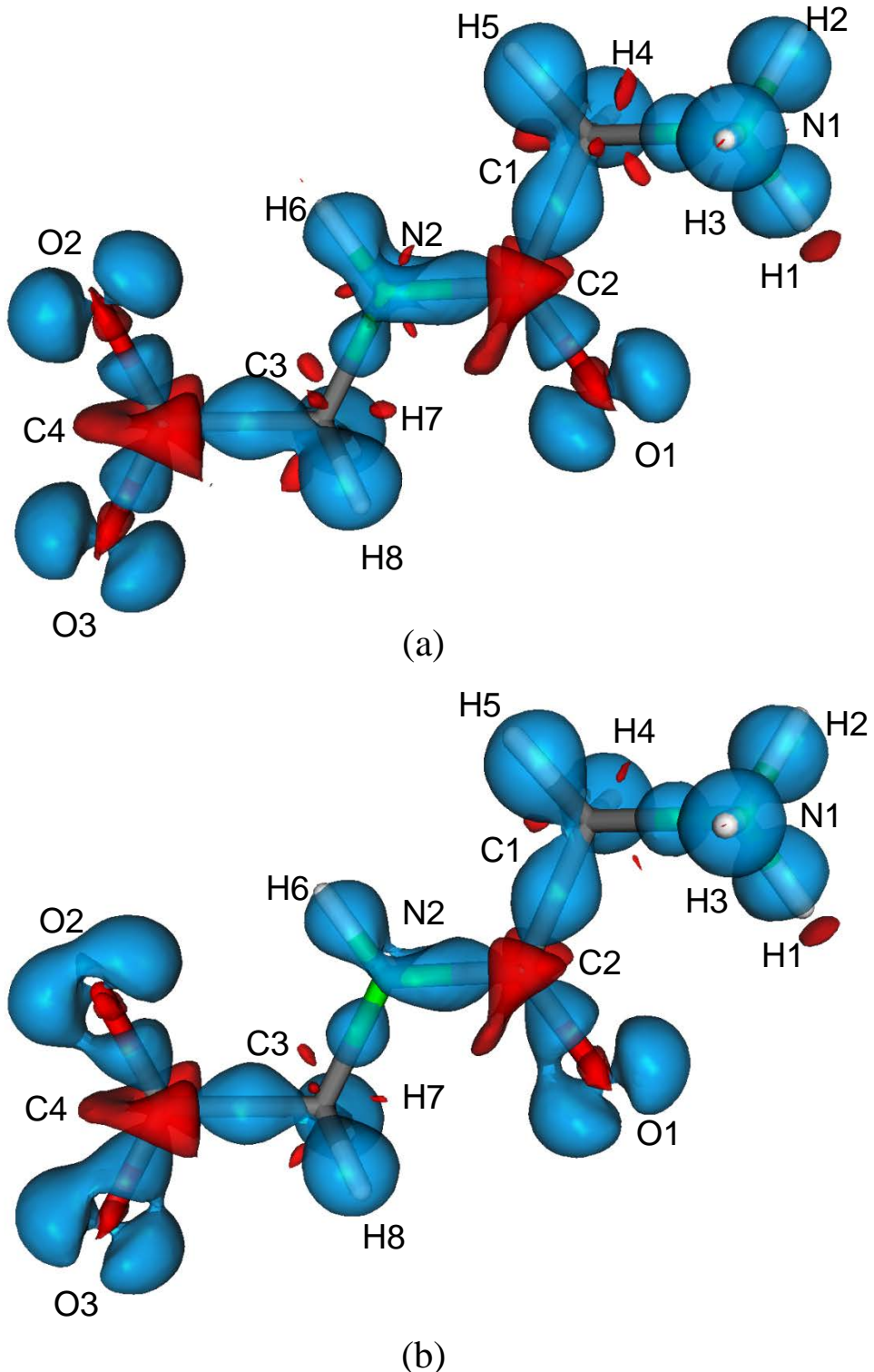
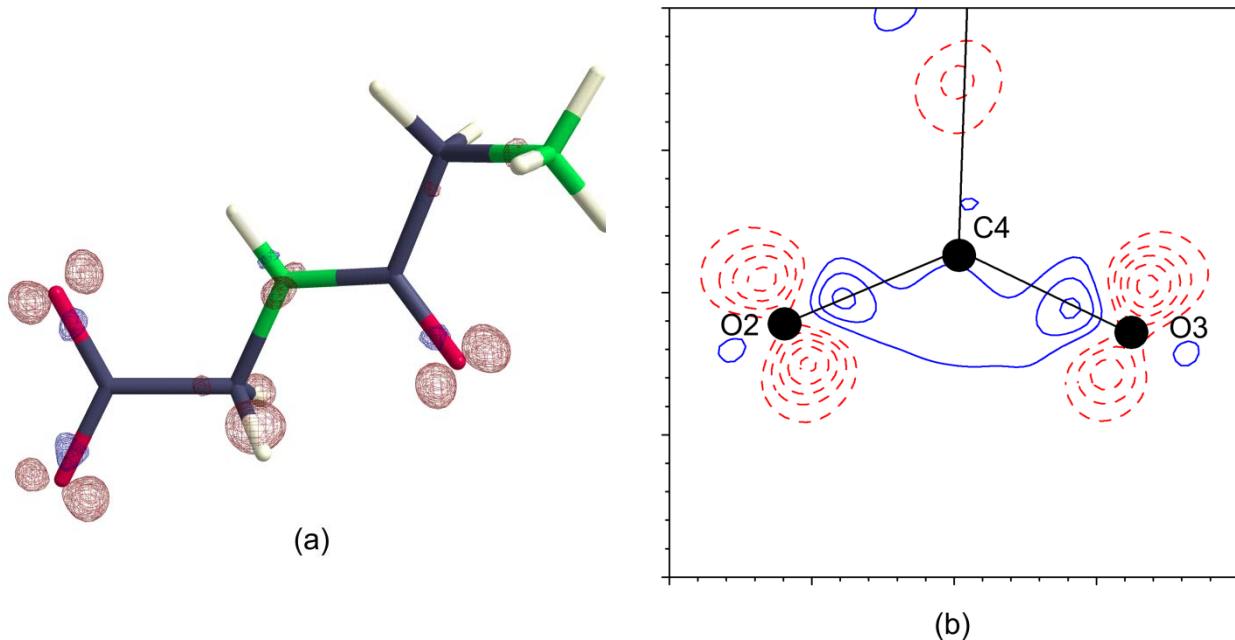


Figure S7. Difference density $\rho^{MM/XC-ELMO} - \rho^{MM/ELMO}$ [6-31G(d,p) basis-set] for glycylglycine. (a) Three-dimensional plot with the isosurface value set to $0.1 \text{ e.}\text{\AA}^{-3}$ and (b) two-dimensional detail of the carboxylate group with contours at linear increments of $0.05 \text{ e.}\text{\AA}^{-3}$. Negative contours are in red and positive contours are in blue.



Here we analyze the effects of the wave function fitting by comparing constrained and unconstrained ELMO/6-31G(d,p) electron density distributions, both projected onto the Hansen & Coppens multipole model. It is possible to note that one of the main fitting consequences is a large redistribution of the electron density around the nuclei, such as the evident depletion of charge in the lone-pairs region of the oxygen atoms. This decrease in electron density is also combined with a simultaneous increase in the charge distribution in the corresponding C–O bonds. Another feature of the fitting is the reduction of electron density in the C3–H7 and C3–H8 bonds. The same effect takes place in the N2–H6 bond, although much less pronounced. Small electron density depletions along the N1–C1, C1–C2 and C3–C4 bonds are also observed.

Table S5. Bond critical point data ^(a) corresponding to all the electron density distributions projected onto the Hansen & Coppens model.

	$\rho^{MM/XC}$	$\rho_{6-31G(2d,2p)}^{MM/P-B3LYP}$	$\rho_{6-31G}^{MM/ELMO}$	$\rho_{6-31G(d,p)}^{MM/ELMO}$	$\rho_{cc-pVDZ}^{MM/ELMO}$	$\rho_{6-31G}^{MM/XC-ELMO}$	$\rho_{6-31G(d,p)}^{MM/XC-ELMO}$	$\rho_{cc-pVDZ}^{MM/XC-ELMO}$
O1–C2								
d_A	0.799	0.796	0.769	0.807	0.809	0.786	0.812	0.812
$\rho(\mathbf{r}_b)$	0.416(4)	0.403	0.385	0.414	0.406	0.386	0.410	0.405
$-\nabla^2\rho(\mathbf{r}_b)$	1.281(7)	1.150	1.160	1.324	1.156	1.129	1.152	1.061
O2–C4								
d_A	0.818	0.802	0.771	0.826	0.825	0.787	0.825	0.824
$\rho(\mathbf{r}_b)$	0.398(4)	0.386	0.367	0.396	0.388	0.366	0.395	0.388
$-\nabla^2\rho(\mathbf{r}_b)$	1.254(7)	1.167	1.094	1.287	1.154	1.075	1.240	1.131
O3–C4								
d_A	0.816	0.803	0.776	0.827	0.825	0.734	0.828	0.823
$\rho(\mathbf{r}_b)$	0.400(4)	0.389	0.372	0.399	0.391	0.375	0.400	0.394
$-\nabla^2\rho(\mathbf{r}_b)$	1.211(7)	1.133	1.119	1.183	1.054	1.094	1.101	0.992
N1–C1								
d_A	0.849	0.841	0.875	0.908	0.923	0.848	0.873	0.884
$\rho(\mathbf{r}_b)$	0.262(3)	0.250	0.224	0.252	0.243	0.234	0.259	0.254
$-\nabla^2\rho(\mathbf{r}_b)$	0.571(3)	0.428	0.269	0.683	0.554	0.318	0.664	0.591
N2–C2								
d_A	0.800	0.778	0.753	0.788	0.794	0.788	0.805	0.813
$\rho(\mathbf{r}_b)$	0.359(3)	0.350	0.340	0.373	0.364	0.337	0.364	0.359
$-\nabla^2\rho(\mathbf{r}_b)$	1.186(4)	1.008	0.850	1.403	1.311	0.962	1.369	1.318

^(a) For each bond critical point (BCP) A–B, d_A is its distance from the nucleus A in Å, $\rho(\mathbf{r}_b)$ is its electron density value in au and $\nabla^2\rho(\mathbf{r}_b)$ is its Laplacian value in au.

Table S5. *Cont.*

N2–C3								
d_A	0.8463	0.820	0.857	0.869	0.881	0.834	0.858	0.867
$\rho(\mathbf{r}_b)$	0.271(3)	0.260	0.236	0.264	0.256	0.252	0.271	0.266
$-\nabla^2\rho(\mathbf{r}_b)$	0.613(3)	0.435	0.312	0.704	0.613	0.409	0.709	0.652
C1–C2								
d_A	0.767	0.772	0.769	0.771	0.771	0.767	0.759	0.762
$\rho(\mathbf{r}_b)$	0.267(2)	0.257	0.245	0.278	0.273	0.242	0.273	0.269
$-\nabla^2\rho(\mathbf{r}_b)$	0.623(2)	0.521	0.454	0.759	0.715	0.426	0.717	0.679
C3–C4								
d_A	0.769	0.768	0.770	0.775	0.778	0.765	0.767	0.767
$\rho(\mathbf{r}_b)$	0.262(2)	0.254	0.245	0.278	0.273	0.242	0.269	0.267
$-\nabla^2\rho(\mathbf{r}_b)$	0.602(2)	0.507	0.468	0.787	0.742	0.432	0.707	0.681
N1–H1								
d_A	0.766	0.759	0.732	0.741	0.749	0.745	0.758	0.767
$\rho(\mathbf{r}_b)$	0.32(2)	0.327	0.328	0.360	0.352	0.318	0.343	0.338
$-\nabla^2\rho(\mathbf{r}_b)$	1.41(3)	1.428	1.239	1.782	1.819	1.247	1.752	1.820
N1–H2								
d_A	0.751	0.745	0.714	0.723	0.731	0.727	0.741	0.749
$\rho(\mathbf{r}_b)$	0.34(2)	0.356	0.345	0.378	0.371	0.338	0.361	0.357
$-\nabla^2\rho(\mathbf{r}_b)$	1.45(3)	1.774	1.270	1.854	1.915	1.345	1.850	1.935
N1–H3								
d_A	0.764	0.760	0.727	0.736	0.743	0.737	0.749	0.757
$\rho(\mathbf{r}_b)$	0.32(2)	0.327	0.324	0.357	0.349	0.325	0.350	0.344
$-\nabla^2\rho(\mathbf{r}_b)$	1.38(2)	1.440	1.078	1.614	1.636	1.208	1.662	1.721

Table S5. *Cont.*

C1–H4								
d_A	0.721	0.717	0.689	0.683	0.673	0.689	0.692	0.685
$\rho(\mathbf{r}_b)$	0.28(2)	0.267	0.266	0.292	0.286	0.272	0.291	0.288
$-\nabla^2\rho(\mathbf{r}_b)$	0.79(2)	0.731	0.653	0.936	0.891	0.713	0.945	0.919
C1–H5								
d_A	0.699	0.693	0.668	0.660	0.649	0.676	0.678	0.671
$\rho(\mathbf{r}_b)$	0.29(2)	0.284	0.280	0.307	0.300	0.277	0.296	0.292
$-\nabla^2\rho(\mathbf{r}_b)$	0.90(2)	0.846	0.750	1.046	0.996	0.724	0.963	0.938
N2–H6								
d_A	0.736	0.730	0.711	0.711	0.716	0.727	0.726	0.732
$\rho(\mathbf{r}_b)$	0.34(2)	0.334	0.334	0.364	0.356	0.331	0.357	0.352
$-\nabla^2\rho(\mathbf{r}_b)$	1.35(3)	1.295	1.102	1.520	1.522	1.272	1.588	1.627
C3–H7								
d_A	0.681	0.679	0.639	0.635	0.621	0.647	0.642	0.633
$\rho(\mathbf{r}_b)$	0.28(2)	0.289	0.295	0.322	0.314	0.288	0.308	0.305
$-\nabla^2\rho(\mathbf{r}_b)$	0.72(2)	0.855	0.816	1.159	1.084	0.805	1.049	1.020
C3–H8								
d_A	0.671	0.648	0.613	0.605	0.590	0.637	0.626	0.617
$\rho(\mathbf{r}_b)$	0.28(2)	0.313	0.314	0.343	0.333	0.289	0.316	0.312
$-\nabla^2\rho(\mathbf{r}_b)$	0.76(2)	1.046	0.976	1.359	1.264	0.804	1.115	1.087

Table S6. Integrated net atomic charges (au) associated with all the electron density distributions projected onto the Hansen & Coppens model.

	$\rho^{MM/XC}$	$\rho_{6-31G(2d,2p)}^{MM/P-B3LYP}$	$\rho_{6-31G}^{MM/ELMO}$	$\rho_{6-31G(d,p)}^{MM/ELMO}$	$\rho_{cc-pVDZ}^{MM/ELMO}$	$\rho_{6-31G}^{MM/XC-ELMO}$	$\rho_{6-31G(d,p)}^{MM/XC-ELMO}$	$\rho_{cc-pVDZ}^{MM/XC-ELMO}$
O1	-1.132	-1.094	-1.026	-1.321	-1.283	-1.164	-1.331	-1.304
O2	-1.184	-1.095	-1.087	-1.387	-1.347	-1.161	-1.343	-1.323
O3	-1.190	-1.108	-1.079	-1.386	-1.345	-1.176	-1.375	-1.355
N1	-1.042	-0.940	-0.812	-0.968	-1.033	-0.851	-1.043	-1.095
N2	-1.034	-0.960	-0.934	-1.121	-1.147	-0.911	-1.129	-1.158
C1	0.158	0.224	0.287	0.439	0.505	0.239	0.336	0.384
C2	1.292	1.223	1.143	1.553	1.548	1.248	1.533	1.537
C3	0.302	0.322	0.416	0.550	0.611	0.363	0.507	0.546
C4	1.618	1.487	1.373	1.979	1.922	1.464	1.866	1.840
H1	0.509	0.452	0.444	0.479	0.498	0.477	0.521	0.539
H2	0.471	0.476	0.401	0.443	0.464	0.439	0.490	0.506
H3	0.484	0.447	0.399	0.432	0.449	0.436	0.474	0.492
H4	0.139	0.091	0.075	0.037	-0.002	0.090	0.076	0.047
H5	0.085	0.061	0.055	0.012	-0.026	0.055	0.042	0.016
H6	0.471	0.419	0.403	0.421	0.432	0.442	0.460	0.471
H7	0.029	0.019	-0.019	-0.067	-0.112	0.014	-0.033	-0.064
H8	0.029	-0.017	-0.032	-0.085	-0.128	0.003	-0.047	-0.074
Σq	0.005	0.007	0.007	0.010	0.006	0.007	0.004	0.005

Table S7. Atomic dipole moment magnitudes (au) associated with all the electron density distributions projected to the Hansen & Coppens model.

	$\rho^{MM/XC}$	$\rho_{6-31G(2d,2p)}^{MM/P-B3LYP}$	$\rho_{6-31G}^{MM/ELMO}$	$\rho_{6-31G(d,p)}^{MM/ELMO}$	$\rho_{cc-pVDZ}^{MM/ELMO}$	$\rho_{6-31G}^{MM/XC-ELMO}$	$\rho_{6-31G(d,p)}^{MM/XC-ELMO}$	$\rho_{cc-pVDZ}^{MM/XC-ELMO}$
O1	0.412	0.294	0.086	0.471	0.409	0.069	0.458	0.406
O2	0.394	0.267	0.121	0.492	0.412	0.097	0.437	0.383
O3	0.431	0.286	0.092	0.522	0.437	0.085	0.520	0.468
N1	0.139	0.147	0.037	0.025	0.034	0.113	0.102	0.146
N2	0.184	0.143	0.065	0.169	0.178	0.151	0.202	0.224
C1	0.465	0.385	0.404	0.441	0.431	0.430	0.434	0.421
C2	0.689	0.646	0.497	0.619	0.616	0.595	0.668	0.671
C3	0.417	0.329	0.371	0.416	0.432	0.296	0.373	0.379
C4	0.720	0.661	0.499	0.643	0.625	0.614	0.702	0.694
H1	0.134	0.159	0.120	0.103	0.111	0.125	0.116	0.121
H2	0.151	0.137	0.124	0.105	0.116	0.134	0.120	0.128
H3	0.148	0.167	0.125	0.109	0.120	0.126	0.118	0.126
H4	0.100	0.139	0.096	0.054	0.054	0.084	0.067	0.065
H5	0.142	0.144	0.105	0.058	0.058	0.121	0.099	0.100
H6	0.130	0.156	0.127	0.103	0.112	0.141	0.117	0.123
H7	0.207	0.199	0.123	0.088	0.084	0.143	0.121	0.116
H8	0.264	0.191	0.124	0.075	0.072	0.185	0.144	0.144

Table S8. Molecular dipole moment magnitudes (au) associated with all the electron density distributions projected onto the Hansen & Coppens model. Bar-graphs are shown in Fig. 9 (b) of the main text.

$\rho^{MM/XC}$	$\rho_{6-31G(2d,2p)}^{MM/P-B3LYP}$	$\rho_{6-31G}^{MM/ELMO}$	$\rho_{6-31G(d,p)}^{MM/ELMO}$	$\rho_{cc-pVDZ}^{MM/ELMO}$	$\rho_{6-31G}^{MM/XC-ELMO}$	$\rho_{6-31G(d,p)}^{MM/XC-ELMO}$	$\rho_{cc-pVDZ}^{MM/XC-ELMO}$
8.408	8.017	9.515	9.655	9.277	9.701	9.613	9.393

Fitting effects on the electrostatic potential

Here we briefly analyze the effects of the X-ray structure factors fitting on electrostatic potentials calculated from the multipole model-projected electron densities. The $\rho^{MM/XC}$ electrostatic potential for glycylglycine is shown in Fig. S8. From the plot is clear that the molecule presents the zwitterionic nature of neutral amino acids, with regions of positive potential around the amino group and slightly negative potential around the carboxylate group. The electrostatic potential is a crucial property for evaluation of intermolecular interaction energetics, playing a key role in molecular recognition processes and in the rational design of molecular crystal structures. However, electrostatic potentials obtained from gas-phase calculations are often significantly different from those obtained from periodic calculations or multipole-projected densities, which emphasizes the importance of lattice environment effects on this property. Therefore, the comparison of electrostatic potentials obtained from the constrained and unconstrained ELMO wave functions with the one calculated from the $\rho^{MM/XC}$ multipole-projected electron density shows the ability of the fitting to recover crystal environment effects and the extent to which the technique is useful to rationally design molecular materials from isolated molecular units. Fig. S9 is the plot of the difference between electrostatic potentials associated with multipole-projected constrained and unconstrained ELMO/6-31G(d,p) electron densities. The difference is generally small (approximately 0.06 e. \AA^{-1}) and mainly concentrated in the carboxylate group, although the differences found in the N2 and C3 regions are also noteworthy.

Figure S8. Glycylglycine electrostatic potential associated with the $\rho^{MM/XC}$ electron density and calculated on the $0.5 \text{ e.}\text{\AA}^{-3}$ charge distribution isosurface. The color gradient scheme ranges from -0.100, red, to 1.500 $\text{e.}\text{\AA}^{-1}$, violet.

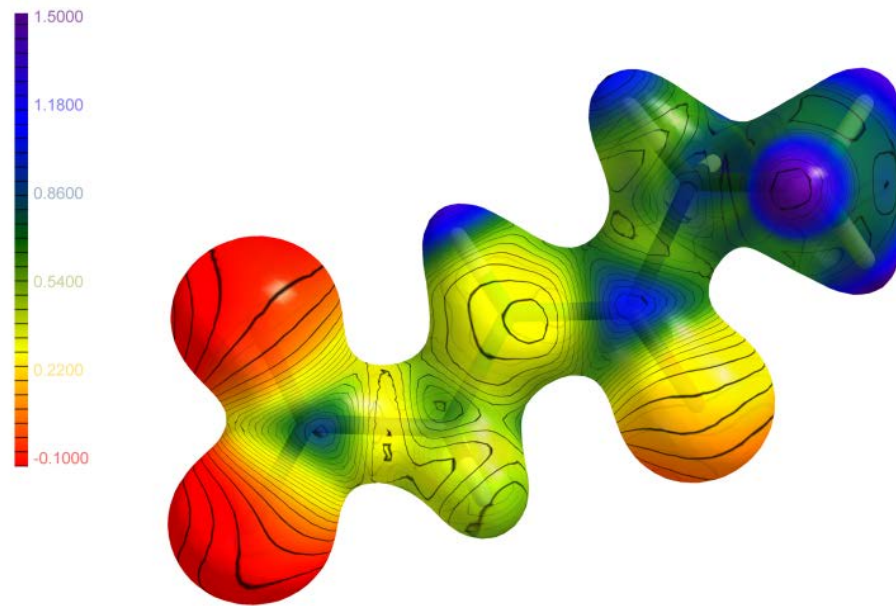


Figure S9. Difference of the electrostatic potentials associated with the $\rho^{MM/XC-ELMO}$ and the $\rho^{MM/ELMO}$ electron distributions [6-31G(d,p) basis-set] plotted on the $0.5 \text{ e.}\text{\AA}^{-3}$ isosurface of the $\rho^{MM/XC}$ electron density. The color gradient scheme ranges from -0.020, red, to 0.070 $\text{e.}\text{\AA}^{-1}$, violet.

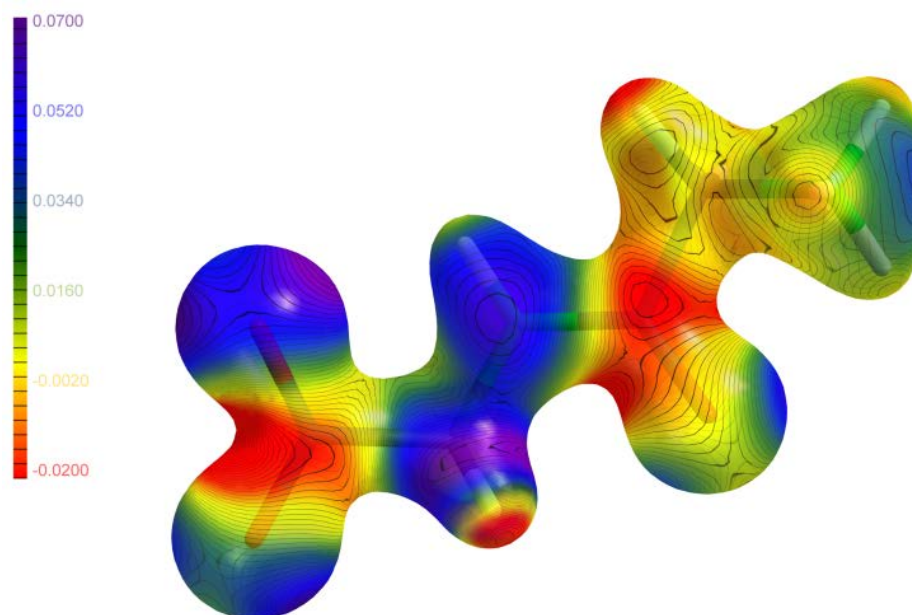


Figure S10. Normalized residuals of the structure factors amplitudes *versus* the scattering resolution for the unconstrained ELMO (a) 6-31G, (b) 6-31G(d,p) and (c) cc-pVDZ wave functions and for the XC-ELMO (d) 6-31G, (e) 6-31G(d,p) and (f) cc-pVDZ wave functions. The calculations use the geometry and, when necessary, ADPs from the Independent Atom Model.

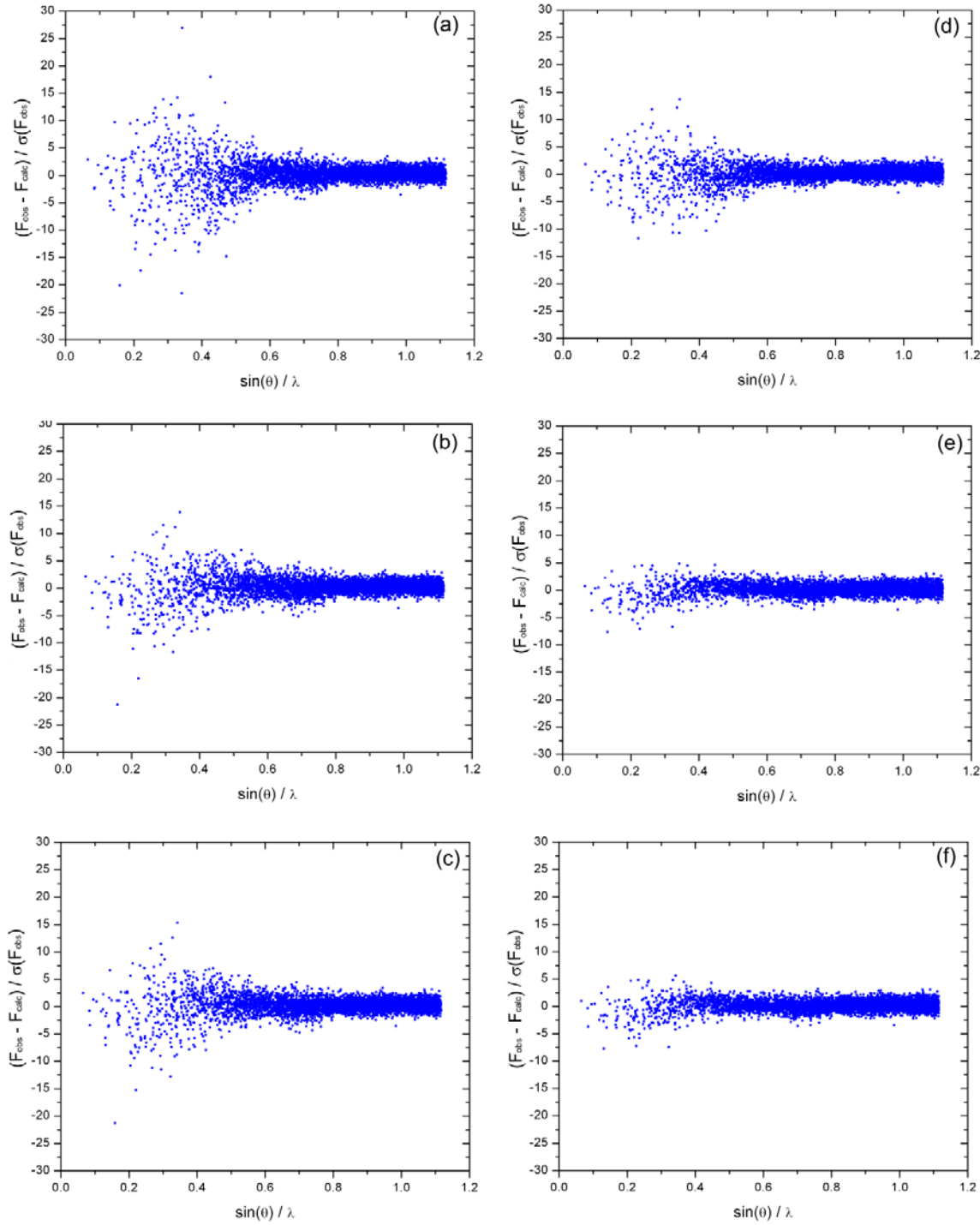


Figure S11. Contour plots of the negative Laplacian in the carboxylate plane of glycylglycine for the (a) $\rho^{MM/XC}$ and (b) $\rho^{MM/P-B3LYP}$ electron distributions. Blue lines denote regions of charge concentration ($L > 0$) and red lines denote regions of charge depletion ($L < 0$).

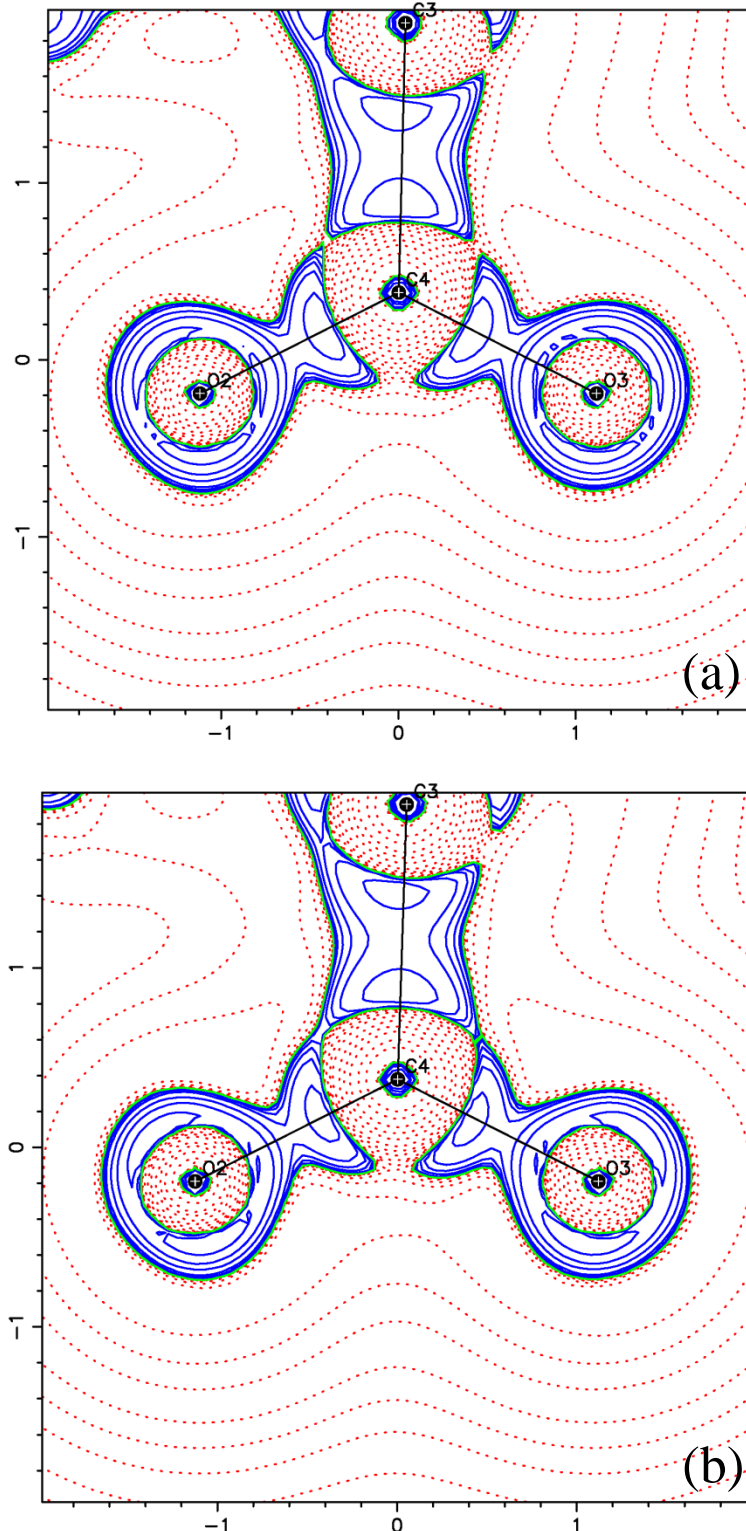


Figure S12. Negative Laplacian associated with the (a) constrained and (b) unconstrained ELMO/6-31G(d,p) wave functions for glycylglycine on a $0.5 \text{ e.}\text{\AA}^{-3}$ electron density isosurface. The color gradient scheme ranges from -3.000, red, to 3.000 $\text{e.}\text{\AA}^{-5}$, violet.

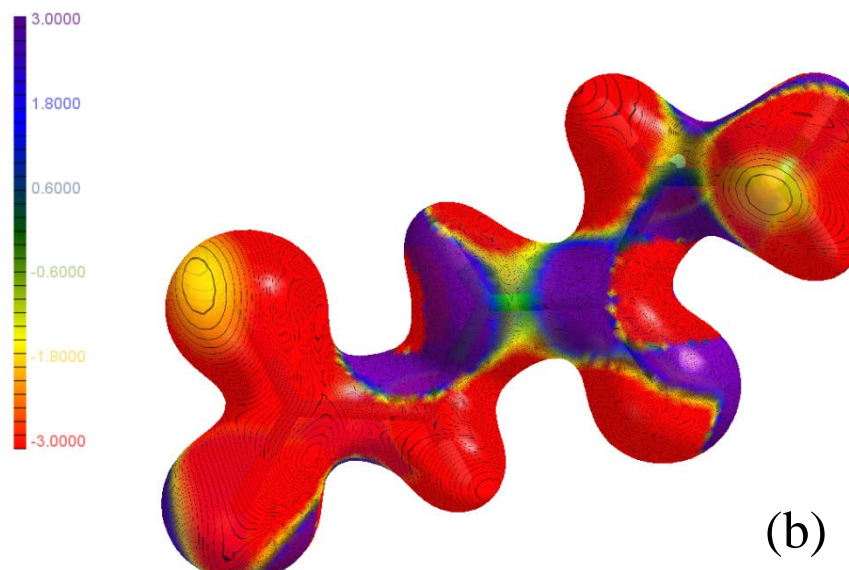
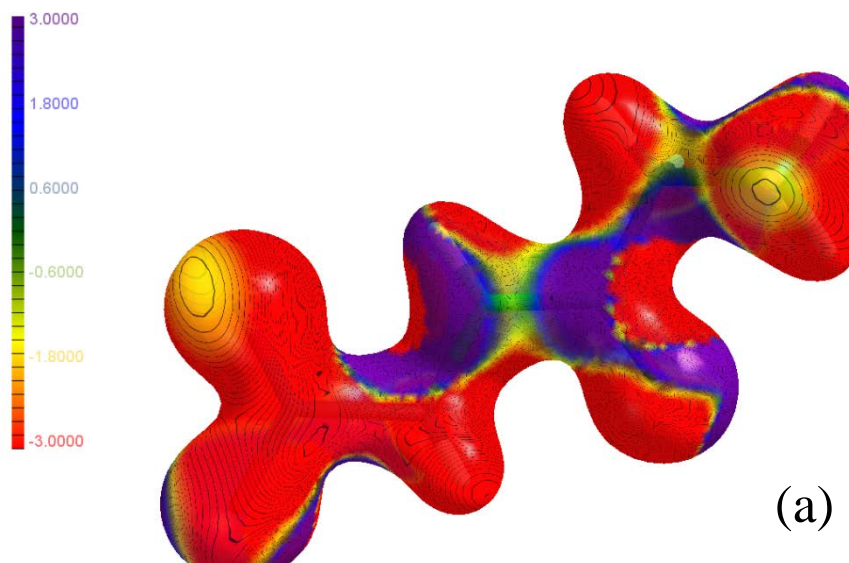


Figure S13. Difference between the negative Laplacian associated with the constrained and the unconstrained ELMO/6-31G(d,p) wave functions for glycylglycine on a $0.5 \text{ e}\cdot\text{\AA}^{-3}$ electron density isosurface. The color gradient scheme ranges from -1.000, red, to 1.000 $\text{e}\cdot\text{\AA}^{-5}$, violet.

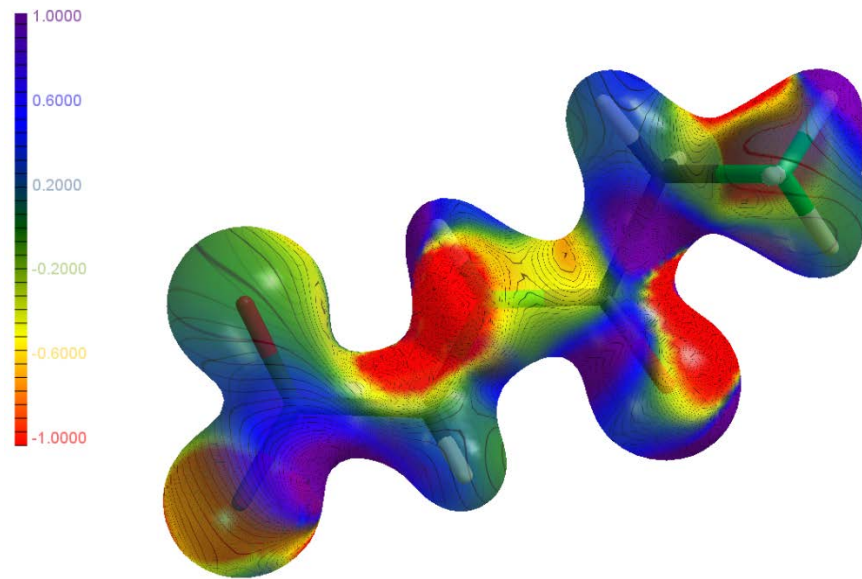


Figure S14. Difference between the negative Laplacian associated with the constrained and the unconstrained ELMO/6-31G(d,p) wave functions for the carboxylate group of glycylglycine at the $3.0 \text{ e}\cdot\text{\AA}^{-5}$ contour level. Blue lines are positive contours and red lines denote negative contours.

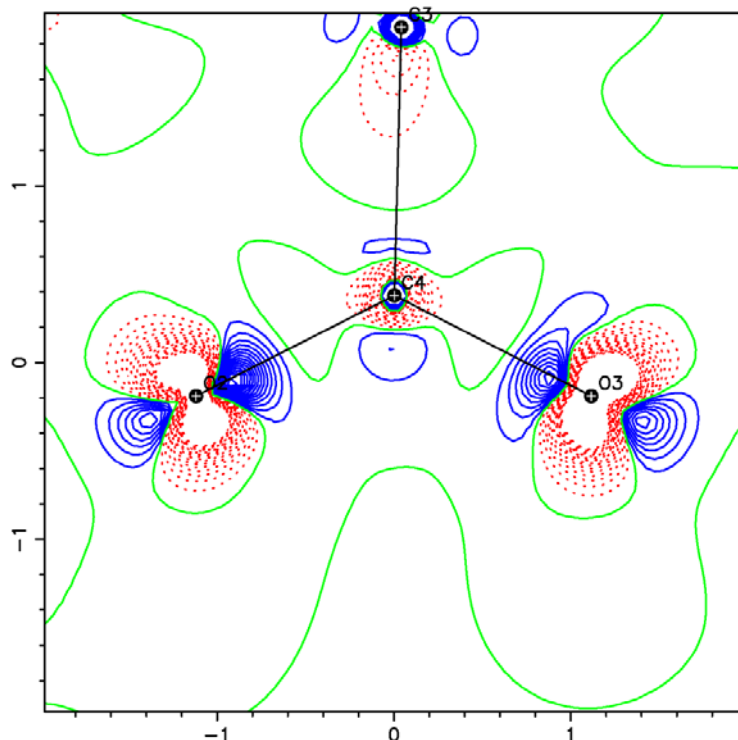


Figure S15. Directions of the atomic dipole moments for glycylglycine from the $\rho^{MM/XC}$ electron distribution.

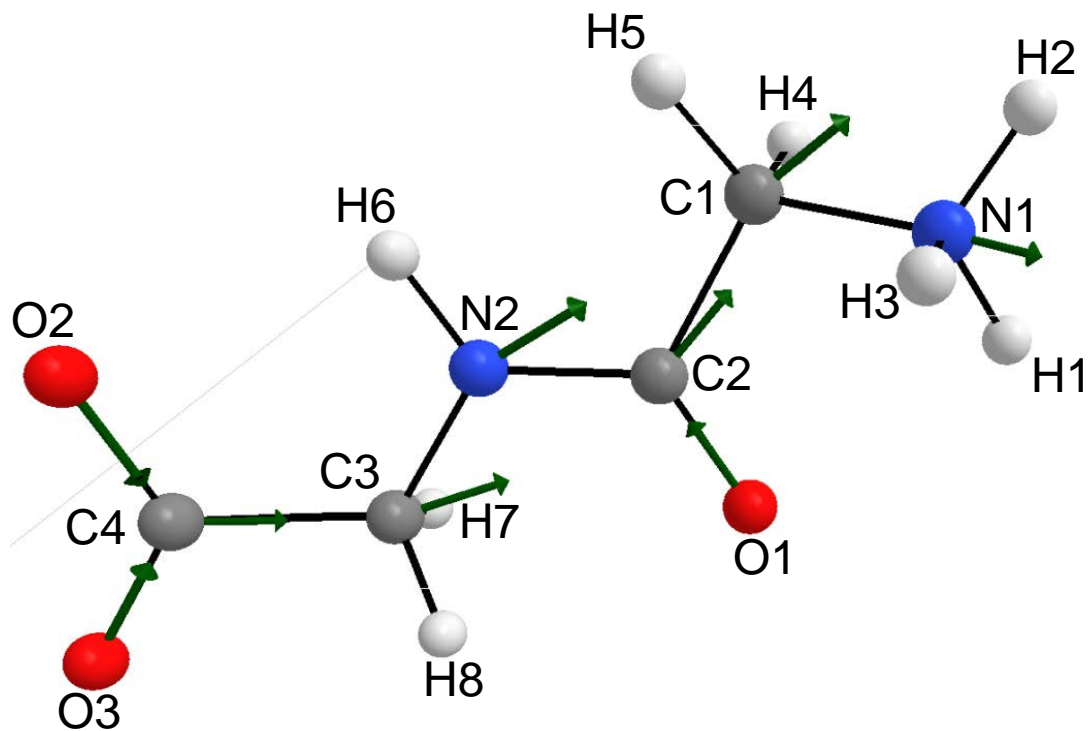


Figure S16. Residual electron density distributions associated with the ELMO and XC-ELMO electron densities. The calculations use the geometry and, when necessary, ADPs from the Multipole Model.

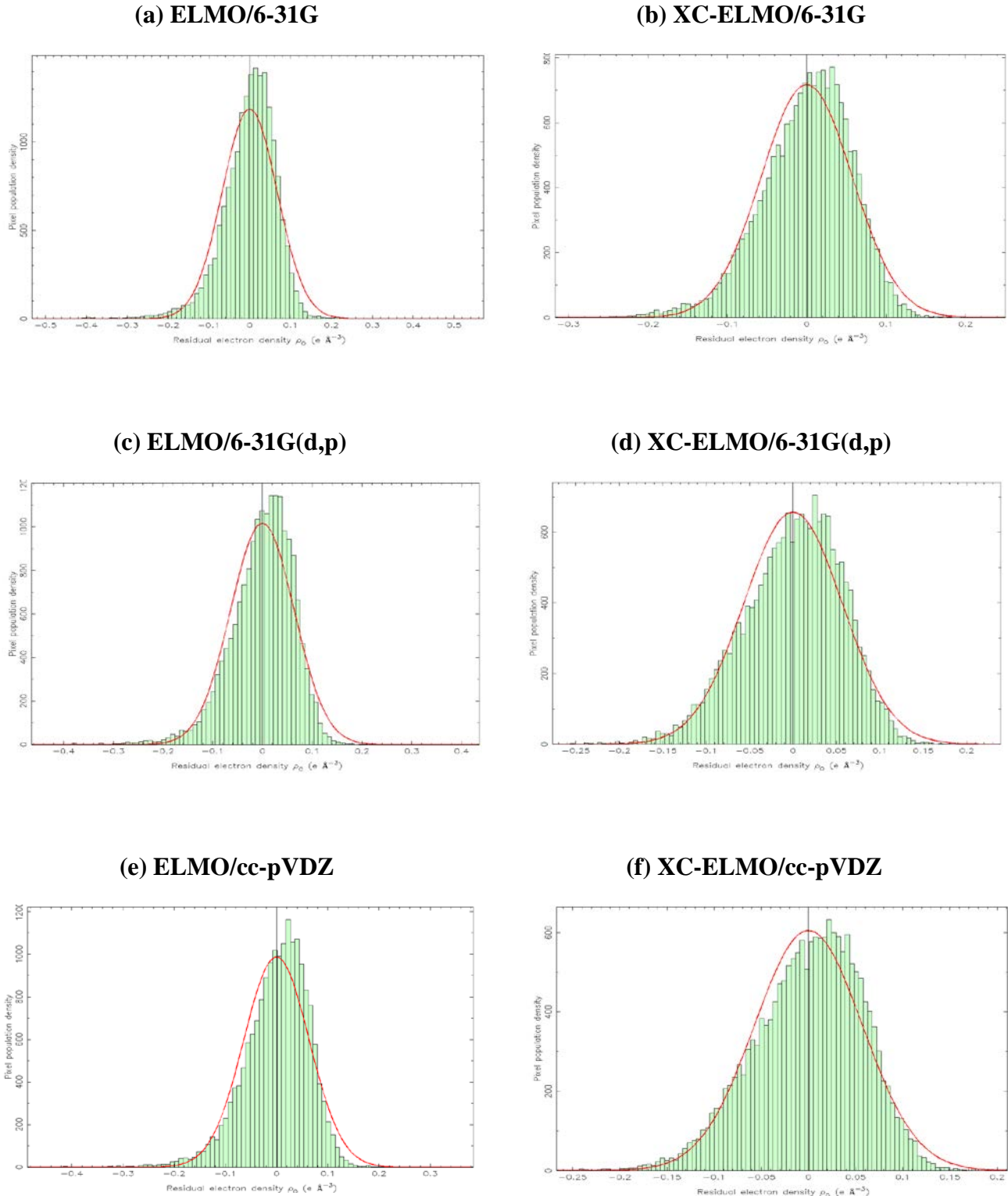


Figure S17. Residual electron density distributions associated with the multipole model-projected ELMO and XC-ELMO electron densities. The calculations use the geometry and, when necessary, ADPs from the Multipole Model.

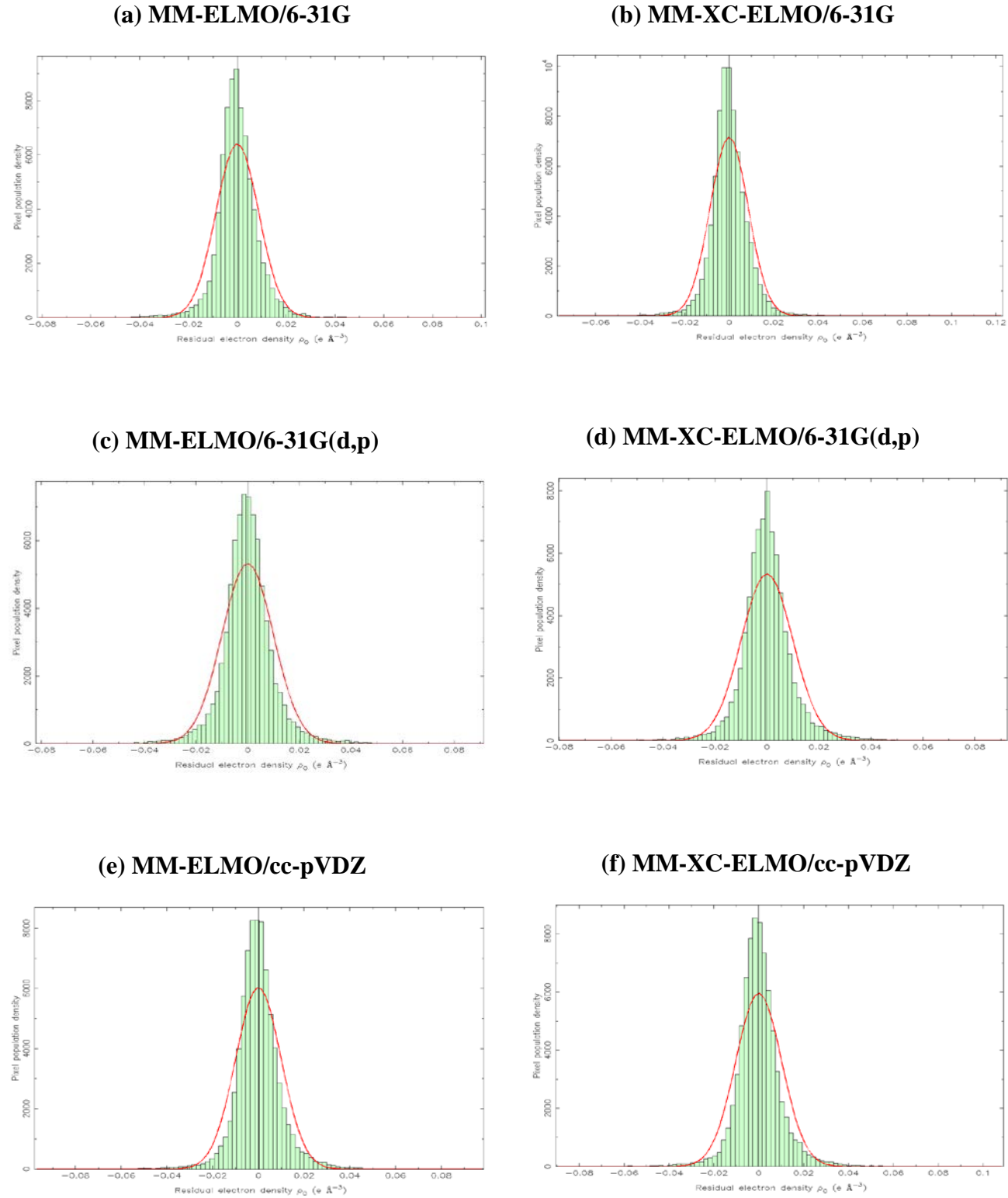


Table S9. Bond critical point data ^(a) for glycylglycine electron densities resulting from unconstrained and constrained Hartree-Fock calculations. Data for the $\rho^{P-B3LYP}$ density are also shown.

	$\rho_{6-31G(2d,2p)}^{P-B3LYP}$	ρ_{6-31G}^{HF}	$\rho_{6-31G(d,p)}^{HF}$	$\rho_{cc-pVDZ}^{HF}$	ρ_{6-31G}^{XC-HF}	$\rho_{6-31G(d,p)}^{XC-HF}$	$\rho_{cc-pVDZ}^{XC-HF}$
O1–C2							
d_A	0.825	0.804	0.834	0.836	0.814	0.835	0.837
$\rho(\mathbf{r}_b)$	0.397	0.380	0.400	0.396	0.379	0.395	0.394
$-\nabla^2\rho(\mathbf{r}_b)$	0.409	0.719	0.097	0.022	0.459	-0.071	-0.063
O2–C4							
d_A	0.837	0.816	0.850	0.851	0.825	0.850	0.851
$\rho(\mathbf{r}_b)$	0.380	0.362	0.381	0.376	0.357	0.378	0.376
$-\nabla^2\rho(\mathbf{r}_b)$	0.532	0.716	0.127	0.095	0.451	0.018	0.051
O3–C4							
d_A	0.834	0.810	0.845	0.846	0.819	0.845	0.846
$\rho(\mathbf{r}_b)$	0.385	0.369	0.388	0.383	0.367	0.387	0.385
$-\nabla^2\rho(\mathbf{r}_b)$	0.519	0.780	0.173	0.134	0.552	0.084	0.106
N1–C1							
d_A	0.879	0.963	1.010	1.001	0.923	0.997	0.977
$\rho(\mathbf{r}_b)$	0.252	0.216	0.239	0.235	0.229	0.248	0.246
$-\nabla^2\rho(\mathbf{r}_b)$	0.642	0.271	0.259	0.309	0.469	0.483	0.558
N2–C2							
d_A	0.836	0.802	0.884	0.876	0.845	0.887	0.883
$\rho(\mathbf{r}_b)$	0.350	0.332	0.358	0.353	0.328	0.350	0.348
$-\nabla^2\rho(\mathbf{r}_b)$	1.282	1.051	1.073	1.182	0.955	0.895	1.025

N2–C3							
d_A	0.874	0.959	0.994	0.988	0.908	0.985	0.973
$\rho(\mathbf{r}_b)$	0.263	0.225	0.246	0.241	0.245	0.256	0.253
$-\nabla^2\rho(\mathbf{r}_b)$	0.712	0.184	0.153	0.210	0.551	0.372	0.477
C1–C2							
d_A	0.747	0.784	0.796	0.799	0.759	0.768	0.769
$\rho(\mathbf{r}_b)$	0.256	0.241	0.272	0.266	0.239	0.269	0.264
$-\nabla^2\rho(\mathbf{r}_b)$	0.560	0.474	0.801	0.723	0.466	0.757	0.695
C3–C4							
d_A	0.757	0.794	0.809	0.815	0.773	0.782	0.787
$\rho(\mathbf{r}_b)$	0.254	0.238	0.268	0.262	0.238	0.263	0.259
$-\nabla^2\rho(\mathbf{r}_b)$	0.551	0.459	0.793	0.706	0.449	0.726	0.660
N1–H1							
d_A	0.808	0.772	0.794	0.800	0.777	0.799	0.803
$\rho(\mathbf{r}_b)$	0.322	0.321	0.353	0.342	0.316	0.339	0.333
$-\nabla^2\rho(\mathbf{r}_b)$	1.849	1.574	2.071	1.888	1.543	1.945	1.866
N1–H2							
d_A	0.785	0.742	0.764	0.769	0.755	0.773	0.776
$\rho(\mathbf{r}_b)$	0.352	0.345	0.378	0.366	0.338	0.360	0.354
$-\nabla^2\rho(\mathbf{r}_b)$	2.083	1.696	2.207	1.970	1.672	2.027	1.924
N1–H3							
d_A	0.804	0.763	0.785	0.792	0.771	0.795	0.801
$\rho(\mathbf{r}_b)$	0.325	0.323	0.355	0.344	0.323	0.344	0.337
$-\nabla^2\rho(\mathbf{r}_b)$	1.873	1.571	2.064	1.829	1.599	1.956	1.834

C1–H4

d_A	0.708	0.696	0.692	0.699	0.702	0.709	0.721
$\rho(\mathbf{r}_b)$	0.269	0.265	0.293	0.288	0.267	0.290	0.286
$-\nabla^2\rho(\mathbf{r}_b)$	0.893	0.801	1.131	1.131	0.817	1.137	1.156

C1–H5

d_A	0.692	0.679	0.674	0.686	0.675	0.682	0.694
$\rho(\mathbf{r}_b)$	0.287	0.280	0.308	0.302	0.281	0.301	0.298
$-\nabla^2\rho(\mathbf{r}_b)$	1.036	0.905	1.259	1.247	0.898	1.194	1.214

N2–H6

d_A	0.789	0.752	0.771	0.776	0.762	0.779	0.782
$\rho(\mathbf{r}_b)$	0.331	0.330	0.360	0.349	0.329	0.352	0.345
$-\nabla^2\rho(\mathbf{r}_b)$	1.899	1.591	2.045	1.795	1.614	1.963	1.833

C3–H7

d_A	0.678	0.641	0.631	0.642	0.646	0.647	0.658
$\rho(\mathbf{r}_b)$	0.289	0.294	0.322	0.314	0.290	0.307	0.304
$-\nabla^2\rho(\mathbf{r}_b)$	1.041	0.992	1.348	1.305	0.982	1.214	1.225

C3–H8

d_A	0.646	0.631	0.621	0.641	0.628	0.625	0.639
$\rho(\mathbf{r}_b)$	0.317	0.312	0.341	0.332	0.295	0.317	0.315
$-\nabla^2\rho(\mathbf{r}_b)$	1.277	1.144	1.523	1.471	1.051	1.305	1.317

^(a) For each bond critical point (BCP) A–B, d_A is its distance from the nucleus A in Å, $\rho(\mathbf{r}_b)$ is its electron density value in au and $-\nabla^2\rho(\mathbf{r}_b)$ is its Laplacian value in au.